

On The Influence of Residual Stresses on Fatigue Fracture of Railway Axles

AUREL RĂDUȚĂ
aurel.raduta@mec.upt.ro

COSMIN LOCOVEI
cosmin.locovei@mec.upt.ro

MIRCEA NICOARĂ
mircea.nicoara@mec.upt.ro

LAURENȚIU ROLAND CUCURUZ
roland.cucuruz@mec.upt.ro

Department of Materials and Manufacturing Engineering,
POLITEHNICA University of Timișoara
Bd. M. Viteazul 1, 300222 Timișoara,
ROMANIA

Abstract: - Influence of residual stresses on the fatigue propagation of cracks represents a major concern for important components subject to complex loading. The purpose of present research is to numerically predict the lifetime of axles used for railway tank wagons in various theoretical conditions. The developed procedure is based on both calculating residual thermal stresses by mean of finite element method, and the number of cycles to fracture, using the closed form solution of NASGRO equation for fatigue. Calculations of fatigue resistance are based on fatigue crack development starting from an initial crack detectable by means of non-destructive testing. The numerical prediction of number of cycles (or kilometers) to fracture for axles belonging to railway tank wagons has proved the deep negative impact of residual thermal stresses introduced by poorly controlled heat treatments or other processing procedures.

Key-Words: - Fatigue fracture, NASGRO equation (Forman–Newman–de Koning equation), Von Misses stresses, Finite element analysis (FEA), Residual thermal stresses, Lifetime prediction.

1 Introduction

Lately, an unprecedented series of major railway axle fractures with many similarities have occurred. Most of the broken axles were from gasoline tank wagons, which usually have higher loads in comparison with passenger wagons. All broken axles were fractured due to the fatigue of material as seen in figure 1 and were manufactured by the same company, the same month.



Figure 1. Broken tank wagon axle from a severe derailment, [1].

Statistics show that in a period of 6 years that has been monitored (1984 – 1989) by Transportation Safety Board (Canada), out of 188 serious derailments only 3 were due to axle failure (approximately 1.56% of total)[2].

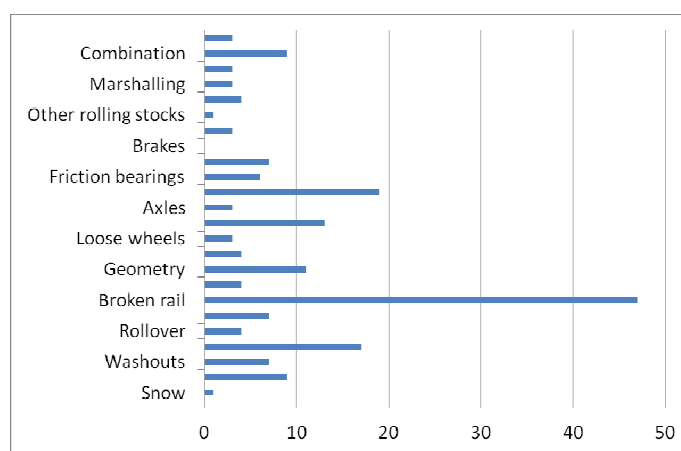


Figure 2. Causes of 188 serious derailments occurred between 1984-1989 in Canada, [2]

Even if the relative number of accidents is small in comparison to other causes of derailments it still remains a real possible cause of accidents and cannot be neglected (figure 2).

Axle failure itself has 2 causes:

- Failure due the fatigue fracture of material. The typical aspect of a broken axle due to the fatigue of material is cylindrical, with flat, relatively smooth fracture surface, with or without shear lips and with generally horizontal marks. Along with ratchet marks (two distinct ratchet marks are evident along the top edge), these features are consistent with reversed bending fatigue, having multiple origins (figure 1)

- Failure due to the overheated roller bearings. Overheated roller bearings occur when inadequate lubrication or mechanical flaws result in an increase of friction inside bearing. This phenomenon is called in railway jargon a “hot box”. The bearing temperature can continue to rise and lead to complete failure of the axle, commonly referred to as a “burnt-off journal”. The typical aspect of a broken axle due to overheated roller bearings is conical (figure 3).

A number of publications provide extensive examples of representative fatigue fractographies [5–9].



Figure 3. View of end cap and remaining portion of axle stub [3].

As expected, the fatigue fracture of the axles has occurred in the area of most intense stresses, below the locking ring (represented in blue) of the bearing (represented in green), as seen in figure 4. In some cases, after the fracture, the wagon continued to run with all the load of the axle supported by the bearing box (represented in red). The heat produced by the intense friction of the axle and the locking ring against the bearing box (figure 5) causes the melt of the locking ring and, ultimately of the bearing box (figure 6 and 7).

After the fracture of the axle, the locking ring of the bearing and the axle continued to jointly rotate, as the locking ring was still supporting the load of the wagon through the bearing box. The load was distributed on a small area of the surface of bearing box and of the locking ring (figure 5).

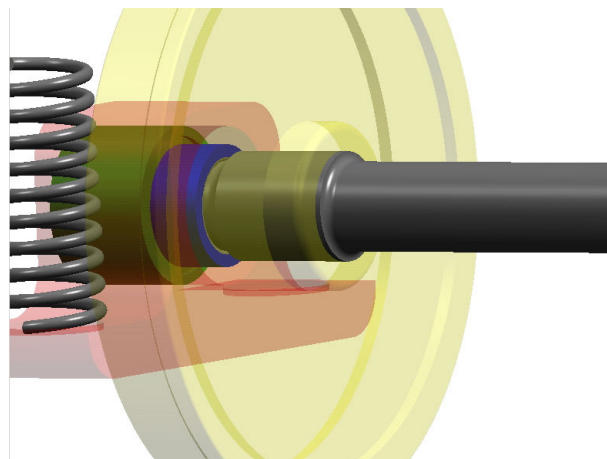


Figure 4. Simplified 3D representation of railway axle.

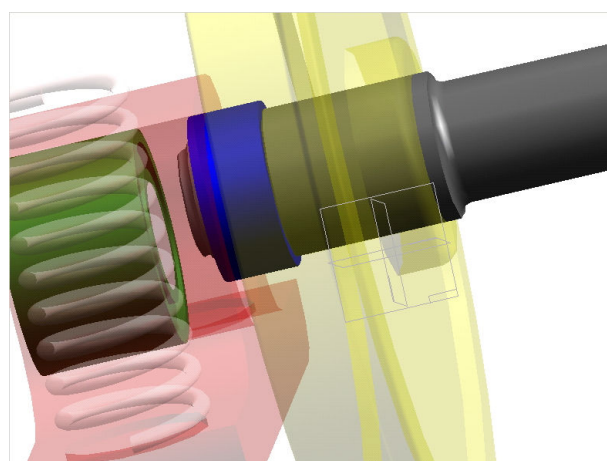


Figure 5. 3D simplified representation of friction of the locking ring against bearing box.

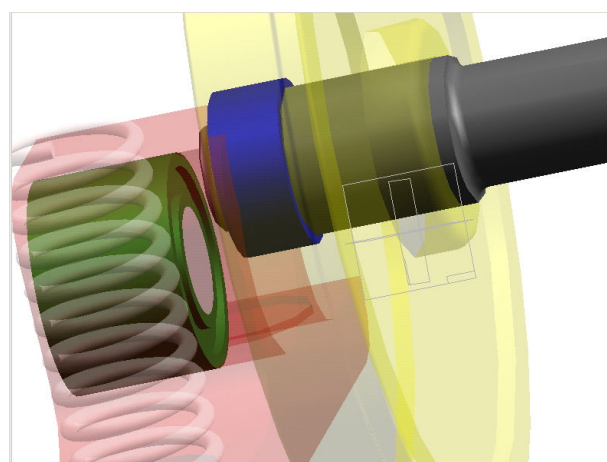


Figure 6. 3D simplified representation of the channel formed as an effect of heat dissipated in the bearing box.

Consequently the heat resulting from the friction was distributed on a small volume of material, causing a rapid augmentation of the temperature. The elevated temperatures caused the decrease of mechanical properties of the material of the bearing box, that lead to the deformation and fracture of bearing box.



Figure 7. The fracture of bearing box as a result of heat dissipated from friction against the locking ring.

The purpose of this article is to numerically simulate the loads, stresses and predict the number of cycles (or kilometers) to fracture in various theoretical conditions. This article does not substitute in any way the legal inquiries (still pending at the time of this article being written) and does not make any assumption or statement regarding the accidents.

2 Methods

An accurate 3D model of the axle has been created using mechanical design software as in figure 8. Restraints and static loads has been applied to this model, in order to numerically calculate von Misses stresses. “No translation” type restraints have been applied to cylindrical surfaces that connect the railway axle to the wheels.

Maximum load of 100 kN has been applied on both ends of the axle. After meshing of 3D model, a static analysis has been performed and von Misses stresses have been calculated. Maximum von Misses stress was 86.27 MPa that is very low in comparison with yield strength of the A1N steel. The deformation scale in figure 9 is 1416.9. The mechanical properties of the material are shown in Table 1.

In order to ensure a much more realistic estimation of stresses in the axle, the dynamic loads have been taken into consideration as a static model [1].

Table 1. Mechanical properties of A1N steel.

Mechanical Properties of A1N steel	Value
Elastic Modulus	210000 N/m
Poissons Ratio	0.26
Shear Modulus	78000 N/m ²
Density	7300 kg/m ³
Ultimate Tensile Strength	550 N/mm ²
Compression Strength	550 N/mm ²
Yield Strength	350 N/mm ²
Thermal Expansion Coefficient	1.5·10 ⁻⁵ /Kelvin
Thermal Conductivity	38 W/(m.K)
Specific Heat	440 J/(kg.K)
Mechanical Properties of A1N steel	Value

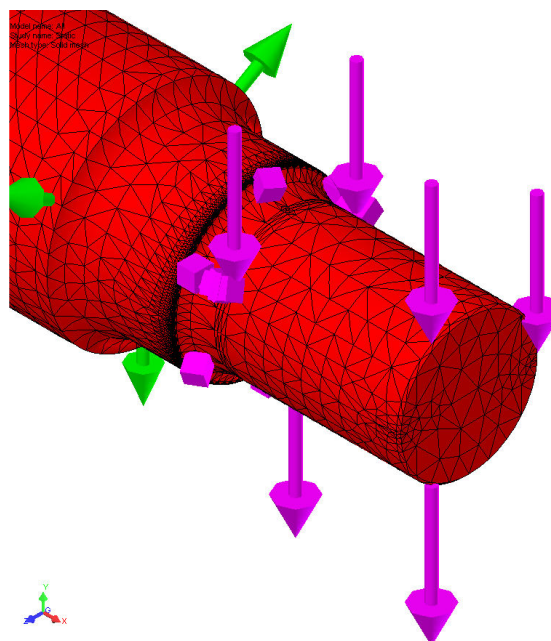


Figure 8. 3D CAD model of tank wagon railway axle.

We have found the maximum von Misses stresses to be 110.7 MPa, a value that is three times lower than the yield strength.

In order to apply the worst case scenario further fracture analyses have been completed right in the section of the axle with maximum von Misses stresses. In addition, other simulations are proposed using residual stresses from a theoretical 5 mm depth welded layer (even such mechanical operations are strictly prohibited by railway regulation. In fact, in railway industry, if a structural moving part does not meet the required dimensions or has material defects (like scratches or cracks) it is

strictly forbidden to cover or repair the part using welding or any other heat treatment).

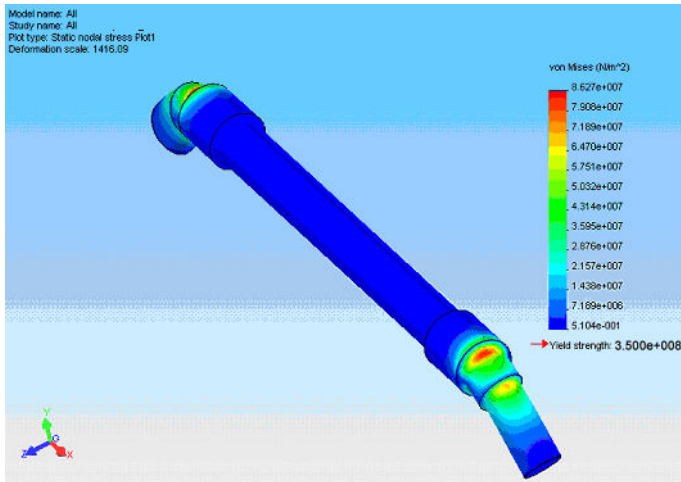


Figure 9. Von Misses stresses and deformations for a tank wagon railway axle model.

These additional simulations were made in order to highlight the real risks of such a procedure. Fracture analyses were completed using NASGRO equation (Eq. 1), expression also called Forman–Newman–de Koning equation jointly introduced by NASA and ESA [4], which is now common in aerospace applications. Equation 1 was numerically solved using AFGROW software.

$$\frac{da}{dN} = C \cdot (\Delta K_{eff})^n \cdot \frac{\left[1 - \frac{\Delta K_0}{\Delta K_{eff}}\right]^p}{\left[1 - \frac{K_{max}}{K_{Jc}}\right]^q} \quad (\text{eq. 1})$$

This equation describes all sections of the da/dN–ΔKeff diagram (figure 10). The term C(ΔKeff)n is fitted to the data in the so-called Paris range (range II) where the curve in the double logarithmic plot constitutes a straight line.

Note, that an upper bound to many empirical curves for steel is provided by reference values to the fit parameters.

$$C = 1.6475 \times 10^{-11} \quad (\text{eq. 2})$$

for da/dN in [m/cycle], K in [Mpa √m] and n = 3.

Due to the fact, that factors such as the mean stress σmed in a load cycle, the stress ratio R and the environment are of minor influence on the curve in range (2) rises the possibility to use reference values for certain material classes such as steels.

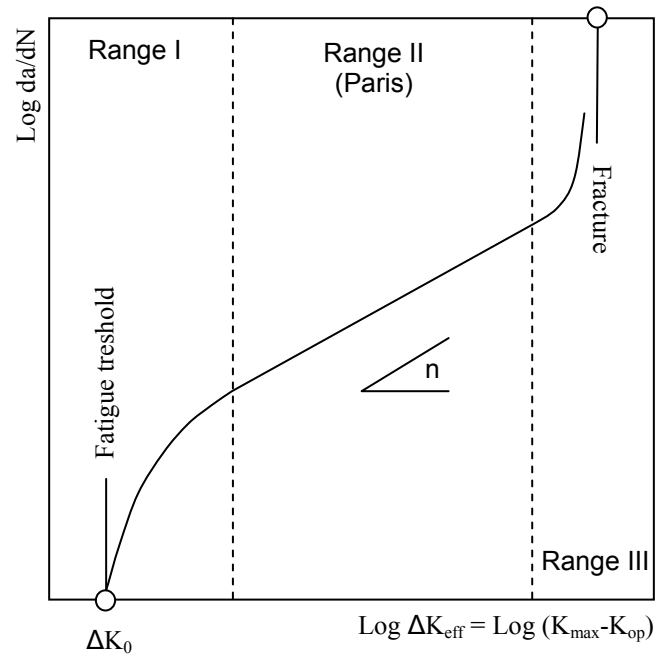


Figure 10. Fatigue crack extension characteristics (da/dN) based on ΔKeff

The same is true with respect to the microstructure of the material. Note, however, that the threshold value ΔK0 shows a strong R-dependence. A conservative threshold value is given in [13] as ΔK0 = 2 MPa √m for steels.

The second and third terms of Eq. (1), $\left[1 - \frac{\Delta K_0}{\Delta K_{eff}}\right]^p$ and

$\left[1 - \frac{K_{max}}{K_{Jc}}\right]^q$ are used for describing range (I) and range

(III) of the overall curve in Fig. 3 with ΔK0 being the fatigue threshold, Kmax maximum stress intensity factor in a load cycle, KJc the crack resistance against fracture and p and q empirical constants from curve fitting. The crack closure concept, the effective stress intensity range ΔKeff is based on as well as the determination of this parameter is described in detail in [11]. Note, that the application of Eq. (1) is restricted to so called “long cracks”. For many practical applications “long cracks” refer to cracks larger than about 2 mm. In practical application, features such as “short cracks”, real load spectra rather than constant amplitude loading, and mixed mode loading of the crack as well as superimposed corrosion often have to be accounted for. In particular variable amplitude loading and mixed mode are common in many railway applications. Whereas the effect of corrosive environments by now can be addressed only by the individual determination of da/dN–ΔKeff curves within the respective media, rules are available for determining the effective stress

intensity range, ΔK_{eff} for variable amplitude and mixed mode loading [12].

The numerical issues involved in crack propagation were further discussed in recent article [10]. The method used by AFGROW is closed form solution, in this particular case; classic model of rod standard solution has been used. The methods in this paper are following the guidelines in recent articles [11] and [12].

3 Results

During AFGROW crack growth simulation the following constants and mechanical material properties were used:

Young's Modulus = 206843

Poisson's Ratio = 0.33

Coeff. of Thermal Expan. = 1.26e-005

The Forman-Newman-de Koning- Henriksen (NASGRO) crack growth relation is being used

No crack growth retardation is being considered

For $Reff < 0.0$, $\Delta K = Kmax$

Material: AlN

Plane strain fracture toughness: 76.919

Plane stress fracture toughness: 115.379

Effective fracture toughness for surface/elliptically shaped crack: 109.884

Fit parameters (KC versus Thickness Equation): $Ak = 0.75$, $Bk = 0.5$

Yield stress: 350

Lower 'R' value boundary: -0.3

Upper 'R' value boundary: 0.8

Exponents in NASGRO Equation: $n = 3.6$, $p = 0.5$, $q = 0.5$

Paris crack growth rate constant: $1.4473e-012$

Threshold stress intensity factor range at $R = 0$: 8.791

Threshold coefficient: 2

Plane stress/strain constraint factor: 2.5

Ratio of the maximum applied stress to the flow stress: 0.5

Failure is based on the current load in the applied spectrum

Vroman integration at 1% crack length

A normalized spectrum was used (figure 11) statistically reproducing the track with straight and curved segments of railway. The spectrum was repeated until fracture has occurred. The load and the initial crack were applied in the section of the axle with maximum stresses.

The following results have been obtained after running the prediction of crack propagation as in Table 2 and figure 12.

For any crack with a depth of less than 5.99 mm the crack will not propagate. The 4.5 mm value was chosen based on probability of non-destructive crack detection.

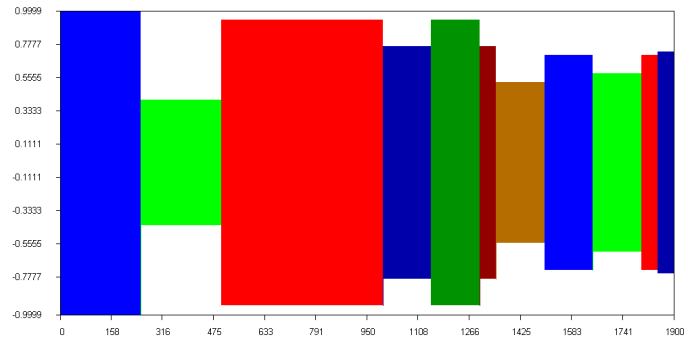


Figure 11. Statistically determined normalized load spectrum.

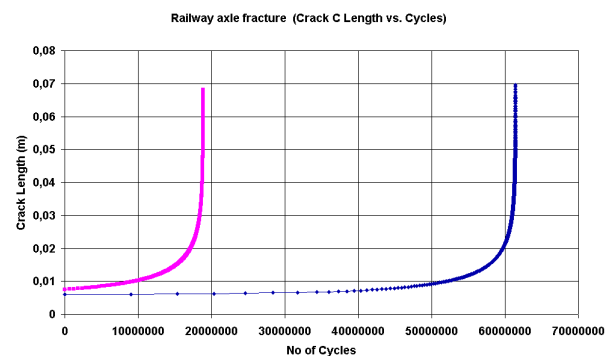


Figure 12. Predictions of crack c lengths [m] against number of cycles for a tank wagon railway axle with no residual stresses starting from different initial crack sizes.

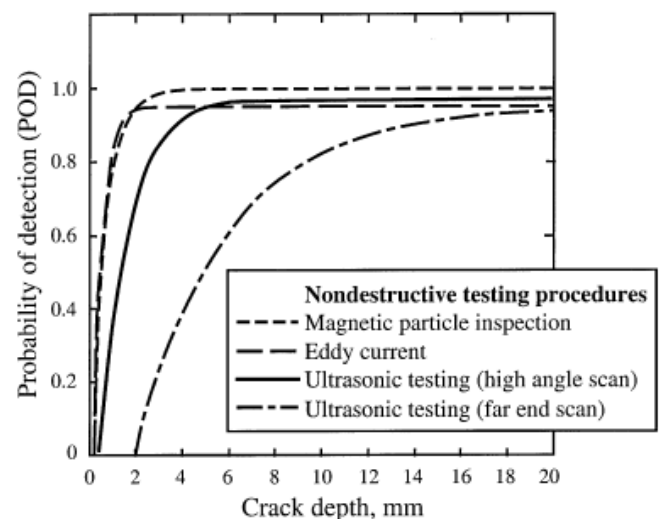


Figure 13. Probability of crack detection in a railway axle as a function of the crack size and various methods of non-destructive inspection [11]

A crack with a 4.5 mm depth is the minimum detectable crack, regardless the non-destructive method applied

[11], with a probability of detection (POD) more than 50% (figure 13).

Table 2. Prediction as number of cycles and kilometres to failure for a tank wagon railway axle fracture with no residual stresses

Initial crack size c [mm]	4.5	6	7.5
Cycles to fracture (no residual stress)	-	$6.1 \cdot 10^7$	$1.8 \cdot 10^7$
Kilometres to fracture (no residual stress)	-	354000	109000

Let assumes that a 5 mm welded layer is laid on external surface of the axle including the section with most elevated stresses. Due to the thermal contraction some residual stresses will appear after the welded layer will cool down (figure 14).

Let us consider:

$$\Delta T = T_{high} - T_{amb} \quad (eq.3)$$

$$\Delta x = x_{high} - x_{amb} \quad (eq.4)$$

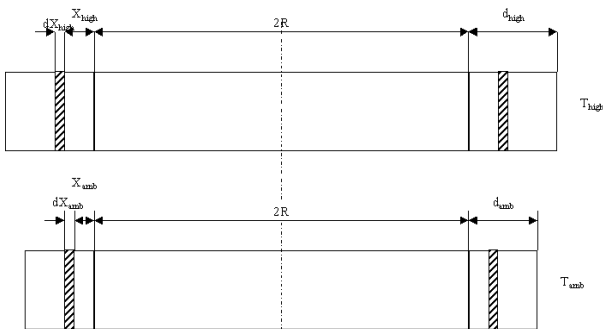


Fig. 14 A theoretical layer of 5 mm at high temperature (T_{high}) and after cooling (T_{amb}) welded on a $2R$ diameter cylinder

Due to the thermal contraction the following equations can be written:

$$x_{amb} = x_{high} (1 - \alpha \cdot \Delta T) \quad (eq.5)$$

$$d_{amb} = d_{high} (1 - \alpha \cdot \Delta T) \quad (eq.6)$$

But, ϵ (relative elongation) can be written as:

$$\epsilon = \frac{\Delta x}{R + x_{high}} \quad (eq.7)$$

Using equations (4) and (5) results:

$$\epsilon = \frac{x_{amb} \cdot \alpha \cdot \Delta T}{R \cdot (1 - \alpha \cdot \Delta T) + x_{amb}} \quad (eq.8)$$

Using Hooke's law the residual stresses can be written as follows:

$$\sigma = E \cdot \epsilon \quad (eq.9)$$

From equations (8) and (9) results:

$$\sigma(x_{amb}) = \frac{E \cdot x_{amb} \cdot \alpha \cdot \Delta T}{R \cdot (1 - \alpha \cdot \Delta T) + x_{amb}} \quad (eq.10)$$

In table 3 are shown residual stresses values for $\Delta T = 200, 400, 600, 800, 1000$ K, at different x_{amb} values or equivalent depth of the new layer [13]. In figure 15 are plotted residual stresses against different values of ΔT and x_{amb} .

Table 3. Calculated residual stresses values[13]

x_{amb}	σ [MPa] at $\Delta T = 400$ K	σ [MPa] at $\Delta T = 600$ K	σ [MPa] at $\Delta T = 800$ K	σ [MPa] at $\Delta T = 1000$ K
0.000	80.57	121.13	161.74	200.48
0.001	65.43	98.38	131.64	165.01
0.002	48.89	75.02	100.24	125.35
0.003	33.77	50.77	67.86	84.79
0.004	17.19	25.85	34.73	43.10
0.005	0.00	0.00	0.00	0.00

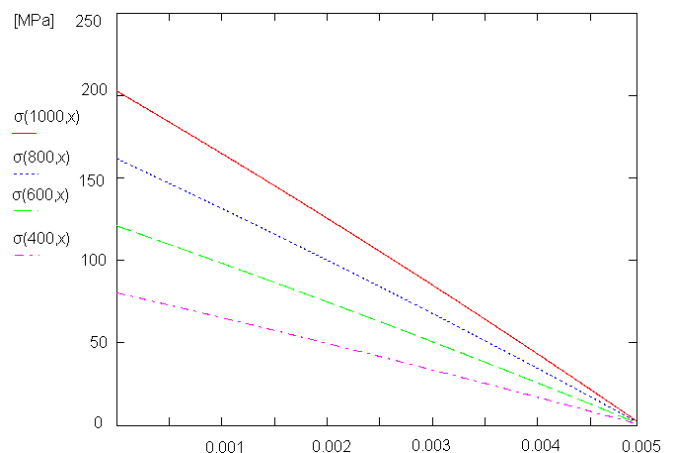


Figure 15. Residual stresses σ [MPa], theoretically calculated, against x [m] and ΔT [K], [13].

In table 4 are shown residual stresses values for $\Delta T = 100$ K, at different x_{amb} values or equivalent depth of the new layer.

Table 4 Calculated residual stresses values for $\Delta T = 100$ K

x_{amb} [m]	σ [MPa]	Depth [m]
0.004994	20.048000	0.000000
0.003994	16.287000	0.001000
0.002998	12.419000	0.001996
0.002012	8.466700	0.002982
0.001006	4.303200	0.003988
0.000000	0.000000	0.004994

In table 5 are shown residual stresses values for $\Delta T = 300$ K, at different x_{amb} values or equivalent depth of the new layer.

Table 5. Calculated residual stresses values for $\Delta T = 300$ K

x_{amb} [m]	σ [MPa]	Depth [m]
0.004981	60.144000	0.000000
0.003994	48.977000	0.000987
0.002998	37.346000	0.001983
0.002002	25.341000	0.002979
0.001006	12.942000	0.003975
0.000000	0.000000	0.004981

In table 6 are shown residual stresses values for $\Delta T = 500$ K, at different x_{amb} values or equivalent depth of the new layer.

Table 6 Calculated residual stresses values for $\Delta T = 500$ K

x_{amb} [m]	σ [MPa]	Depth [m]
0.004968	100.239000	0.000000
0.003999	81.917000	0.000969
0.002993	62.296000	0.001975
0.002007	42.440000	0.002961
0.001001	21.519000	0.003967
0.000000	0.000000	0.004968

In table 7 are shown residual stresses values for $\Delta T = 700$ K, at different x_{amb} values or equivalent depth of the new layer.

Table 7 Calculated residual stresses values for $\Delta T = 700$ K

x_{amb} [m]	σ [MPa]	Depth [m]
0.004956	140.340000	0.000000
0.003999	114.960000	0.000957
0.003003	87.701000	0.001953
0.001997	59.277000	0.002959
0.001006	30.349000	0.003950
0.000000	0.000000	0.004956

Also, a mean value of residual stresses (σ_{med}) can be calculated using:

$$\sigma_{med} = \frac{1}{d_{amb}} \int_0^{d_{amb}} \frac{E \cdot \alpha \cdot \Delta T \cdot x_{amb} \cdot dx_{amb}}{R \cdot (1 - \alpha \cdot \Delta T) + x_{amb}} \quad (eq.11)$$

Using eq.(11) the following mean residual stresses has been calculated (table 8):

Table 8 Calculated mean residual stresses

ΔT [K]	σ_{med} [MPa]
700	71.40
600	61.28
500	51.13
400	40.96
300	30.76
200	20.53
100	10.28

Using residual stresses calculated for $\Delta T = 100, 300, 500$ and 700 K (tables 4 to 7), new predictions regarding crack propagation were made. As expected, the number of cycles to failure dramatically decreases with the increase of residual stresses (ΔT increases).

If in the axle there are residual stresses due a thermal contraction of welded material with $\Delta T = 100$ K than any crack with a depth of less than 1.50 mm will not propagate. Prediction as number of cycles to failure and as a number of kilometers to failure for a tank wagon railway axle fracture with residual stresses due to a thermal contraction of welded material at $\Delta T = 100$ K are presented in tables 9 and 10 and figures 16 and 17.

Table 9. Prediction as number of cycles to failure for a tank wagon railway axle fracture with residual stresses due to a thermal contraction of welded material at $\Delta T = 100$ K

Initial crack depth size c [mm]	Cycles to fracture
1.50 mm	16824152
2.00 mm	7467000
4.50 mm	2714422

Table 10. Prediction as number of kilometers to failure for a tank wagon railway axle fracture with residual stresses due to a thermal contraction of welded material at $\Delta T = 100$ K

Initial crack depth size c [mm]	kilometers to fracture
1.50 mm	47 569
2.00 mm	21 112
4.50 mm	7 674

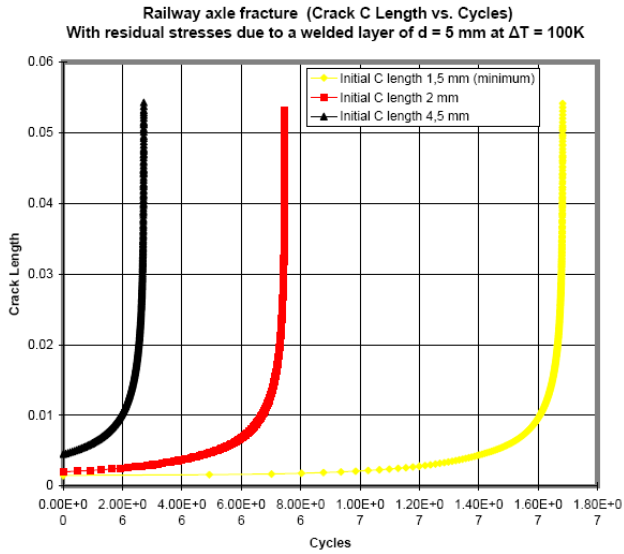


Figure 16. Prediction of crack c length [m] vs. Cycles with residual stresses due to a welded layer of $d = 5$ mm at $\Delta T = 100K$ for a tank wagon railway axle

If in the axle there are residual stresses due a thermal contraction of welded material with $\Delta T = 300$ K than any crack with a depth of less than 0.83 mm will not propagate.

Prediction as number of cycles to failure and as a number of kilometers to failure for a tank wagon railway axle fracture with residual stresses due to a thermal contraction of welded material at $\Delta T = 300$ K are presented in tables 11 and 12 and figures 18 and 19.

Table 11. Prediction as number of cycles to failure for a tank wagon railway axle fracture with residual stresses due to a thermal contraction of welded material at $\Delta T = 300$ K

Initial crack depth size c [mm]	Cycles to fracture
0.83 mm	13695200
2.00 mm	3777261
4.50 mm	2184261

Table 12. Prediction as number of kilometers to failure for a tank wagon railway axle fracture with residual stresses due to a thermal contraction of welded material at $\Delta T = 300$ K

Initial crack depth size c [mm]	kilometers to fracture
0.83 mm	38 722
2.00 mm	10 679
4.50 mm	6 175

If in the axle there are residual stresses due a thermal contraction of welded material with $\Delta T = 500$ K than any crack with a depth of less than 0.76 mm will not propagate. Prediction as number of cycles to failure and as a number of kilometers to failure for a tank wagon railway axle fracture with residual stresses due to a thermal contraction of welded material at $\Delta T = 500$ K are presented in tables 13 and 14 and figures 20 and 21.

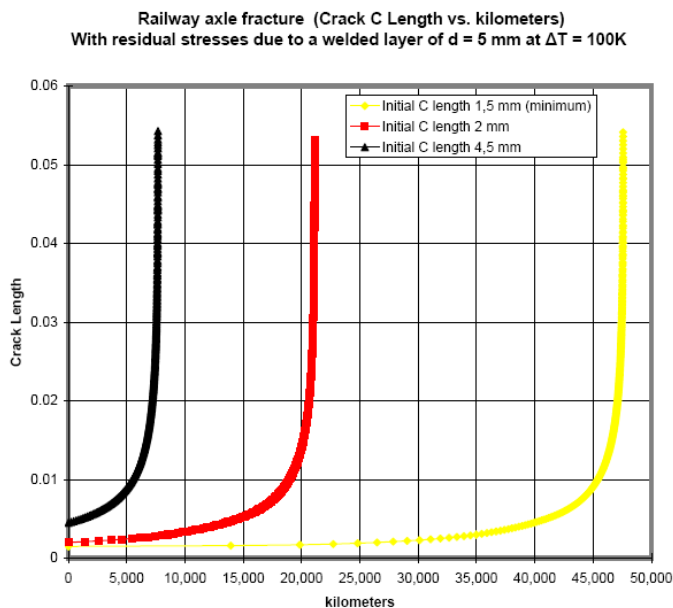


Figure 17. Prediction of crack c length [m] vs. kilometers with residual stresses due to a welded layer of $d = 5$ mm at $\Delta T = 100K$ for tank wagon railway axle

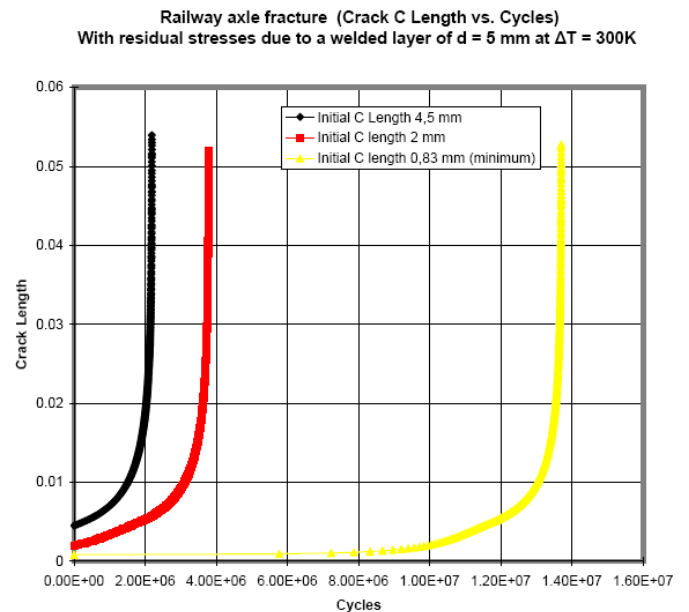


Figure 18. Prediction of crack c length [m] vs. Cycles with residual stresses due to a welded layer of $d = 5$ mm at $\Delta T = 300K$ for a tank wagon railway axle

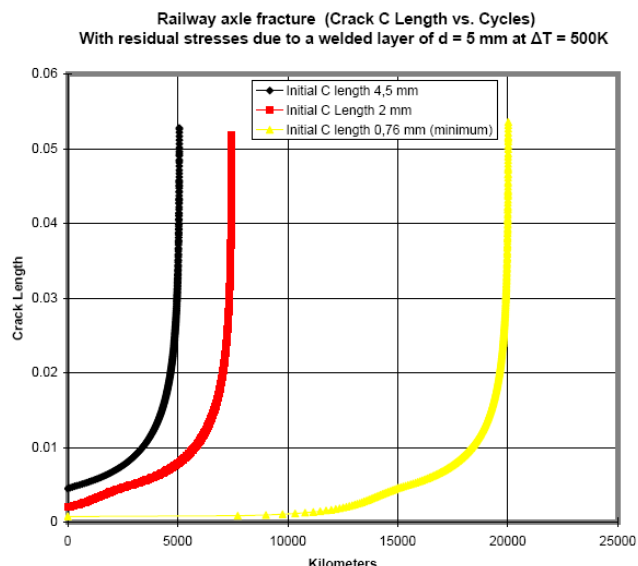


Fig. 19. Prediction of crack c length [m] vs. kilometers with residual stresses due to a welded layer of $d = 5$ mm at $\Delta T = 300K$ for a tank wagon railway axle

Table 13. Prediction as number of cycles to failure for a tank wagon railway axle fracture with residual stresses due to a thermal contraction of welded material at $\Delta T = 500$ K

Initial crack depth size c [mm]	Cycles to fracture
0.76 mm	7080500
2.00 mm	2633585
4.50 mm	1793600

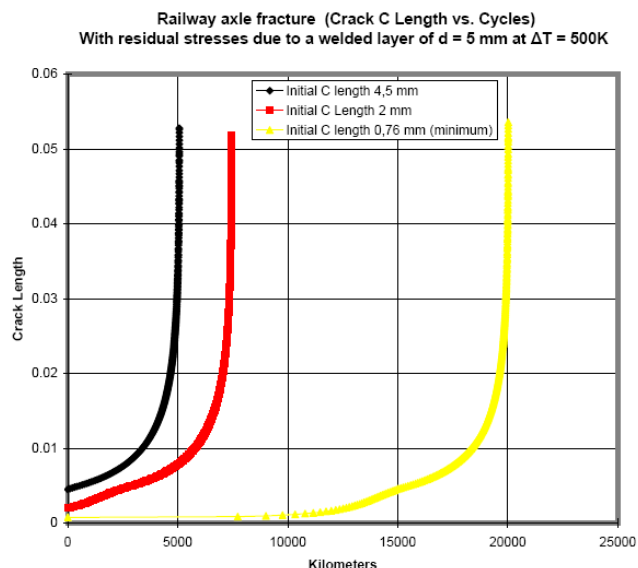


Figure 20. Prediction of crack c length [m] vs. kilometers with residual stresses due to a welded layer of $d = 5$ mm at $\Delta T = 500K$ for tank wagon railway axle

Table 14. Prediction as number of kilometers to failure for a tank wagon railway axle fracture with residual stresses due to a thermal contraction of welded material at $\Delta T = 500$ K

Initial crack depth size c [mm]	kilometers to fracture
0.76 mm	20 019
2.00 mm	7 446
4.50 mm	5 071

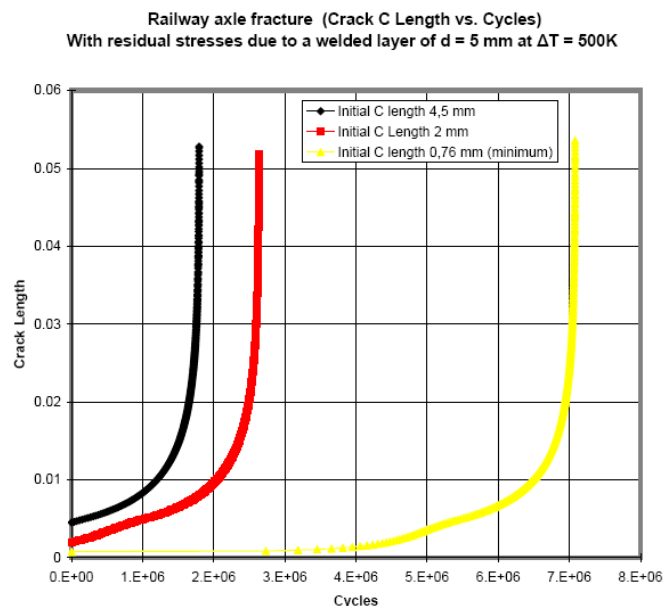


Fig. 21. Prediction of crack c length [m] vs. cycles with residual stresses due to a welded layer of $d = 5$ mm at $\Delta T = 500K$ for a tank wagon railway axle

Table 15. Prediction as number of cycles to failure for a tank wagon railway axle fracture with residual stresses due to a thermal contraction of welded material at $\Delta T = 700$ K

Initial crack depth size c [mm]	Cycles to fracture
0.61 mm	4991300
1.99 mm	2011420
4.50 mm	1493582

Table 16. Prediction as number of kilometers to failure for a tank wagon railway axle fracture with residual stresses due to a thermal contraction of welded material at $\Delta T = 700$ K

Initial crack depth size c [mm]	kilometers to fracture
0.61 mm	14 112
1.99 mm	5 687
4.5 mm	4 223

If in the axle there are residual stresses due a thermal contraction of welded material with $\Delta T = 700$ K than any crack with a depth of less than 0.61 mm will not propagate.

Prediction as number of cycles to failure and as a number of kilometers to failure for a tank wagon railway axle fracture with residual stresses due to a thermal contraction of welded material at $\Delta T = 700$ K are presented in tables 15 and 16 and figures 22 and 23.

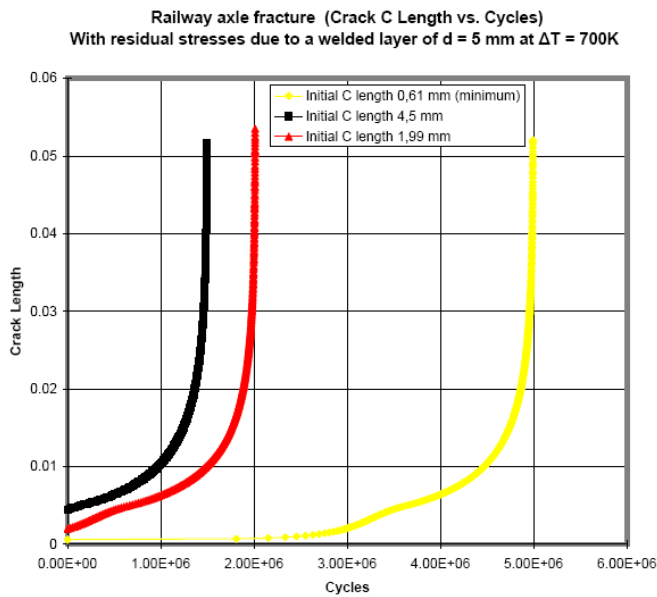


Fig. 22. Prediction of crack c length [m] vs. Cycles with residual stresses due to a welded layer of $d = 5$ mm at $\Delta T = 700$ K for a tank wagon railway axle

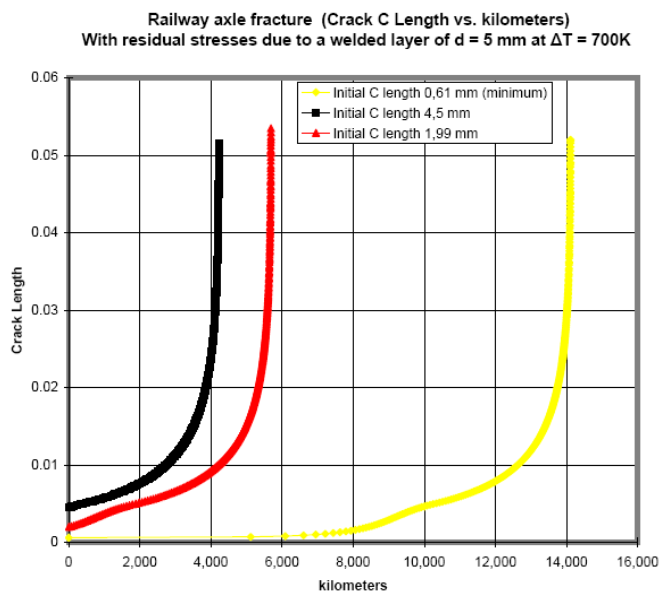


Fig. 23. Prediction of crack c length [m] vs. kilometers with residual stresses due to a welded layer of $d = 5$ mm at $\Delta T = 700$ K for a tank wagon railway axle

5 Conclusions

Any residual stresses in a railway axle will dramatically reduce the number of cycles (kilometers) to failure (figure 24).

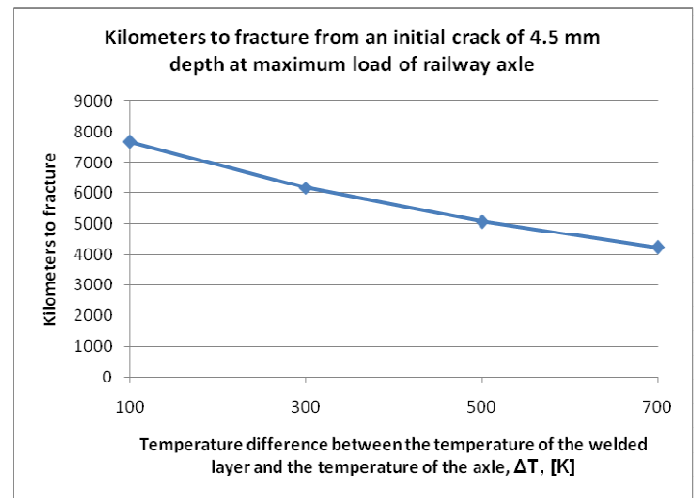


Fig. 24. Prediction of kilometers to failure from an initial crack of 4.5 mm for a tank wagon railway axle without or with residual stresses due to a welded layer of $d = 5$ mm at $\Delta T = 100$ K, 300K, 500K, 700K.

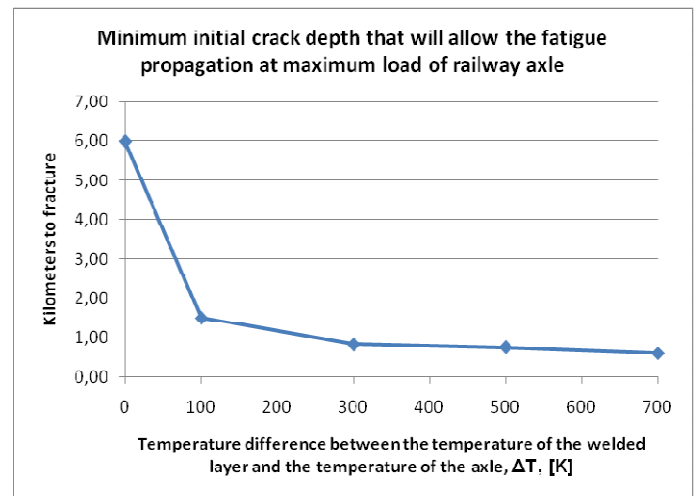


Fig. 25. Prediction of minimum initial crack depth that will allow fatigue propagation of the crack for a tank wagon railway axle without or with residual stresses due to a welded layer of $d = 5$ mm at $\Delta T = 100$ K, 300K, 500K, 700K.

Any residual stresses in a railway axle will also, dramatically reduce the minimal initial crack depth in order to propagate the crack (figure 25).

In real life the railway axle will not fracture as soon as predicted in this paper for a few reasons:

- Wagons will not always be filled (sometimes they have to be emptied);

- If there is no residual stress, a corrosion crack will grow very slowly to a depth that will propagate through fatigue, in a longer period than the time needed to fracture the axle through fatigue propagation. But, it is probable and plausible that a crack will develop in a welded layer right from the beginning;
- A worst case scenario was used, the crack was supposed to be right in the section of the maximum stresses.
- Residual stresses should not be present in a railway axle.

References:

- [1] A. Raduta, M. Nicoara, C. Locovei, C.T. Demian, *Technical expertise regarding the nature and the causes of railway axles failure* (2005), "Politehnica" University of Timișoara, Romania.
- [2] Transportation Safety Board of Canada, *TRANSPORTATION IN CANADA 1992*, Annual Report.
- [3] Talamba, R., Stoica, M., (2005) In "OSIA MONTATĂ" (Mounted Axle), pp. 240 – 246, (Ed.) Editura ASAB, Bucuresti, Romania.
- [4] NASGRO. (2000) *Fatigue Crack Growth Computer Program*, NASGRO, version 3, NASA, L.B. Johnson Space Centre, Houston, Texas. JSC-22267B.
- [5] Fractography, Vol 12, Metals Handbook,(9th ed.), ASM International, 1987
- [6] S. Bhattacharyya, V.E. Johnson, S. Agarwal, and M.A.H. Howes, *Failure Analysis of Metallic Materials by Scanning Electron Microscopy*, IITRI Fracture Handbook, IIT Research Institute, 1979
- [7] L. Engel and H. Klingele, *An Atlas of Metal Damage*, Prentice-Hall, 1981
- [8] G.W. Powell, S. Cheng, and C.E. Mobley, Jr., *A Fractography Atlas of Casting Alloys*, Battelle Press, 1992
- [9] J. Aleszka, Y. Kim, J. Scott, and A. Kumar, *Fracture Characteristics of Structural Steels: Reference Manual*, U.S. Army Construction Engineering Research Laboratory Technical Report M-258, 1979
- [10] C. Timbrell, R. Chandwani, G.Cook, *Journée Scientifique 2004: Les méthodes de dimensionnement en fatigue*, Centre de Compétences Matériaux & Conception (CCM&C), Fribourg, Switzerland, Oct 27 2004.
- [11] U.Zerbst, M.Vormwald, C. Andersch, K. Mädler, M. Puff, , *Engineering Fracture Mechanics* **72** (2005), pp. 209–239.
- [12] U. Zerbst, C. Mädler, H. Hintze, *Engineering Fracture Mechanics* **72**(2005), pp. 163-194.
- [13] A. Raduta, M. Nicoara, C. Locovei, C.T. Demian, *Scientific Bulletin of the "Politehnica" University of Timisoara*, Transactions on Mechanics Special issue (2005), pp. 75-87
- [14] S. Boljanovic, S. Maksimovic, I. Belic, *Total Fatigue Life of Structural Components*, Proceedings of the 2nd WSEAS Int. Conference on Applied and Theoretical Mechanics, Venice, Italy, November 20-22, 2006, pp 1-6
- [15] N. Gubeljak1, M. Cvetic, J. Predan, A. Poles, M. Madercic, M. Oblak, *Structure Integrity Assessment of a Windflow Power Plant's Axle*, Proc. of the 9th WSEAS Int. Conf. on Mathematical and Computational Methods in Science and Engineering, Trinidad and Tobago, November 5-7, 2007, pp. 74-78
- [16] K. Krishnapillai, R. Jones, *Fatigue based 3D structural design optimisation implementing genetic algorithms and utilising the generalised Frost-Dugdale crack growth law*, Proc. of the 9th WSEAS Int. Conf. on Mathematical and Computational Methods in Science and Engineering, Trinidad and Tobago, November 5-7, 2007, pp. 119-125
- [17] A. Savaidis, G. Tsamasphyros, G. Savaidis, M. Vormwald, *Mode I fatigue crack growth evaluation at notches*, 6th WSEAS International Conference on SYSTEM SCIENCE and SIMULATION in ENGINEERING, Venice, Italy, November 21-23, 2007, pp. 387-392